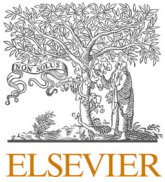




Since January 2020 Elsevier has created a COVID-19 resource centre with free information in English and Mandarin on the novel coronavirus COVID-19. The COVID-19 resource centre is hosted on Elsevier Connect, the company's public news and information website.

Elsevier hereby grants permission to make all its COVID-19-related research that is available on the COVID-19 resource centre - including this research content - immediately available in PubMed Central and other publicly funded repositories, such as the WHO COVID database with rights for unrestricted research re-use and analyses in any form or by any means with acknowledgement of the original source. These permissions are granted for free by Elsevier for as long as the COVID-19 resource centre remains active.



## Research paper

## Development of antibody-based assays for high throughput discovery and mechanistic study of antiviral agents against yellow fever virus



Zhao Gao<sup>a</sup>, Lin Zhang<sup>a</sup>, Julia Ma<sup>a</sup>, Andrea Jurado<sup>b</sup>, Seon-Hui Hong<sup>b</sup>, Ju-Tao Guo<sup>a</sup>, Charles M. Rice<sup>b</sup>, Margaret R. MacDonald<sup>b</sup>, Jinhong Chang<sup>a,\*</sup>

<sup>a</sup> Baruch S. Blumberg Institute, Hepatitis B Foundation, Doylestown, PA, USA

<sup>b</sup> The Laboratory of Virology and Infectious Disease, The Rockefeller University, New York, NY, USA

## ARTICLE INFO

**Keywords:**

Yellow fever virus  
Antibody  
Antiviral assay  
High throughput screening  
Antiviral

## ABSTRACT

Despite the availability of a highly effective yellow fever virus (YFV) vaccine, outbreaks of yellow fever frequently occur in Africa and South America with significant mortality, highlighting the pressing need for antiviral drugs to manage future outbreaks. To support the discovery and development of antiviral drugs against YFV, we characterized a panel of rabbit polyclonal antibodies against the three YFV structural proteins and five non-structural proteins and demonstrated these antibody reagents in conjunction with viral RNA metabolic labeling, double-stranded RNA staining and membrane floatation assays as powerful tools for investigating YFV polyprotein processing, replication complex formation, viral RNA synthesis and high throughput discovery of antiviral drugs. Specifically, the proteolytic processing of the viral polyprotein can be analyzed by Western blot assays. The predominant nuclear localization of NS5 protein as well as the relationship between intracellular viral non-structural protein distribution and foci of YFV RNA replication can be revealed by immunofluorescence staining and membrane flotation assays. Using an antibody against YFV NS4B protein as an example, in-cell western and high-content imaging assays have been developed for high throughput discovery of antiviral agents. A synergistic antiviral effect of an YFV NS4B-targeting antiviral agent BDAA and a NS5 RNA-dependent RNA polymerase inhibitor (Sofosbuvir) was also demonstrated with the high-content imaging assay. Apparently, the antibody-based assays established herein not only facilitate the discovery and development of antiviral agents against YFV, but also provide valuable tools to dissect the molecular mechanism by which the antiviral agents inhibit YFV replication.

## 1. Introduction

Yellow fever is a mosquito-borne disease caused by yellow fever virus (YFV) infection and frequently associated with a severe form of hemorrhagic fever and liver injury with jaundice leading to a mortality rate of up to 60% (Monath and Vasconcelos, 2015). YFV infection can be prevented by the attenuated 17D vaccine and its derivatives (Klitting et al., 2018a, 2018b). The combination of vector-control and vaccination campaigns has significantly reduced the incidence of YFV infection in the human population. However, the virus remains in a sylvatic cycle between mosquito vectors and nonhuman primates and can occasionally transmit to humans through mosquito bites. This results in tremendous difficulty to manage the disease, not only at individual and local levels, but also globally. Concern has been raised regarding the possibility of yellow fever taking hold in previously unaffected and unvaccinated

parts of the world such as Asia, where host, vector, and climatic conditions could conspire to promote YFV dissemination.

In 2016, there were urban yellow fever outbreaks in Angola and Democratic Republic of Congo, which resulted in vaccine shortage and emergent vaccination campaigns using only one-fifth of the regular vaccine dosage in high-risk populations (Calisher and Woodall, 2016). In late 2017 and early 2018, there was another urban outbreak in Brazil. While the number of yellow fever cases are significantly underreported due to the undeveloped nature of many endemic areas, it is estimated that up to 1.7 million YFV infections occur in Africa each year resulting in 29,000–60,000 deaths (Douam and Ploss, 2018). This outnumbers the estimated death toll of global dengue virus infection (<http://www.who.int/mediacentre/factsheets/fs100/en/>). The World Health Organization and its partners responded to these recent outbreaks of yellow fever and emphasized the importance of additional research and the development

\* Corresponding author.

E-mail address: [jinhong.chang@bblumberg.org](mailto:jinhong.chang@bblumberg.org) (J. Chang).

of new vaccines, diagnostics and therapeutics as countermeasures (<http://www.who.int/emergencies/yellow-fever/response/en/>).

While improvement of vaccines and vaccination policy remains the best strategy to control global yellow fever endemics and epidemics, it is anticipated that other yellow fever outbreaks will occur in the near future. Therefore, it is crucial to develop safe and highly efficacious antiviral strategies against YFV infection that can be used not only for treating infected patients, but also for the prophylactic treatment of individuals potentially exposed to YFV, since sufficient post-vaccination immunity requires at least a week to develop (Douam et al., 2018; Gaucher et al., 2008; Querec et al., 2009). Moreover, a safe antiviral therapy would be invaluable for visitors to endemic/epidemic regions who cannot safely take the attenuated vaccine (e.g., seniors and immunocompromised individuals). Presently, there is no antiviral drug available for the treatment and/or prevention of yellow fever (Beasley et al., 2015; Douam and Ploss, 2018; Julander, 2013).

Over the past decades, tremendous industrial and academic efforts have been made toward the discovery and development of vaccines and antiviral agents against emerging flaviviruses such as dengue virus (DENV), Japanese encephalitis virus (JEV), and Zika virus (ZIKV) (Lim et al., 2013). However, research on the molecular virology and pathogenesis of YFV, as well as development of novel vaccines and antiviral agents, have lagged largely due to the unrealistic assumption that current vaccination strategies would be sufficient to prevent and ultimately eliminate the disease. Improving yellow fever management through the development of effective therapeutics will require in-depth understanding of the molecular biology and pathogenesis of YFV, knowledge of which remains surprisingly limited given YFV's medical significance.

Like other flaviviruses, YFV has a single positive-strand RNA genome approximately 11 kb in length with a 5' cap but no 3'-polyA tail. The genome encodes a polyprotein that is co-translationally processed by viral and host cellular proteases into three structural proteins (i.e., capsid (C), membrane (prM/M), envelope (E)) and seven non-structural (NS) proteins (i.e., NS1, NS2A, NS2B, NS3, NS4A, NS4B, NS5) (Douam and Ploss, 2018; Lescar et al., 2018). Few reagents and research tools, particularly the antibodies against YFV proteins, are available for investigating the molecular mechanism of YFV replication and pathogenesis. Currently, the commercially available YFV antibodies are only limited to the envelope and NS1 proteins. A couple of epitope-mapped monoclonal antibodies specific for YFV envelope or NS1 protein were reported, but have not been made available commercially (Adungo et al., 2016; Ricciardi-Jorge et al., 2017). Polyclonal antibodies against capsid and NS1 have been developed as well, which were proposed for use in YFV research and for the development of novel diagnostic tests (Stock et al., 2015). Taking advantage of the recently available rabbit polyclonal antibodies against all three YFV structural proteins and five of the seven non-structural proteins (i.e., NS1, NS2B, NS3, NS4B and NS5) from GeneTex, Inc., we established several antibody-based assays and demonstrated their utility, in conjunction with viral RNA metabolic labeling, double stranded RNA staining and membrane floatation assays, in molecular and cellular analyses of viral proteins and RNA synthesis in YFV infection, antiviral drug discovery and mechanistic studies.

## 2. Materials and methods

### 2.1. Cell lines and viruses

Vero cells were purchased from ATCC. Huh-7 and Huh-7.5 cells (Blight et al., 2002) were cultured in DMEM, 10% fetal bovine serum (FBS), 1X non-essential amino acid (NEAA). The 293TLR3/IFN $\beta$ Luc cell line was established based on HEK293 (ATCC) with reconstituted TLR3 as well as an interferon  $\beta$  promotor driven luciferase, as previously described (Guo et al., 2014). Yellow fever virus 17D strain was generated from a cDNA clone, pACNR/FLYF-17Dx (Bredenbeek et al., 2003; Guo et al., 2016; Rice et al., 1985). Yellow fever virus Asibi strain was generated from a slightly modified version of plasmid

**Table 1**  
Summary of YFV antibodies from GeneTex, Inc.

| YFV Antibody      | Catalog No. | Immunogen  |
|-------------------|-------------|--|
| Capsid antibody   | GTX134022   | Full-length capsid recombinant protein   |
| prM antibody      | GTX133957   | Peptide encompassing a sequence within the center region of prM                  |
| Envelope antibody | GTX134024   | Recombinant protein encompassing a sequence within the center region of envelope |
| NS1 antibody      | GTX134025   | Recombinant protein encompassing a sequence within the center region of NS1      |
| NS1 antibody      | GTX134026   | Recombinant protein encompassing a sequence within the C-terminus region of NS1  |
| NS2B antibody     | GTX134028   | Full-length NS2B recombinant protein   |
| NS3 antibody      | GTX133958   | Peptide encompassing a sequence within the C-terminus region of NS3              |
| NS3 antibody      | GTX133959   | Peptide encompassing a sequence within the center region of NS3                  |
| NS4B antibody     | GTX134030   | Recombinant protein encompassing a sequence within the center region of NS4B     |
| NS5 antibody      | GTX134141   | Recombinant protein encompassing a sequence within the N-terminus region of NS5  |

pACNR-FLYF-Asibi (Yi et al., 2011), designated pACNR-2015FLYF-Asibi, the sequence of which has been deposited to GenBank (MT093734). The modifications were based on a comparison of the plasmid sequence to that of Asibi sequences available in GenBank and included three nucleotide changes (nucleotide 6013 was changed from C to T, 6829 from T to C, and 8008 from C to T) to more accurately reflect the Asibi sequence.

### 2.2. Antibodies

All the YFV protein-specific rabbit polyclonal IgG antibodies were provided by GeneTex, Inc. These antibodies were raised by immunizing rabbits with synthetic peptides or recombinant proteins (Table 1). The antibodies were purified from rabbit sera by antigen-affinity chromatography. Anti-Flavivirus Group Antigen antibody 4G2 was purchased from EMD Millipore. J2 double-stranded RNA (dsRNA) mouse monoclonal antibody was purchased from English & Scientific Consulting, Szirak, Hungary. Mouse monoclonal antibodies against  $\beta$ -actin and Hsp70 were purchased from Cell Signaling Technology. Mouse monoclonal antibodies against calnexin was obtained from GeneTex. Alexa Fluor Goat anti-Mouse 488 IgG (H + L) and Alexa Fluor Goat anti-Rabbit 594 IgG (H + L) were purchased from Invitrogen. IRDye® 800CW Goat anti-Mouse and anti-Rabbit antibodies, and IRDye 680RD Goat anti-Mouse IgG were purchased from LI-COR.

### 2.3. Western blot assay

YFV 17D infected cells were lysed with 1  $\times$  NuPAGE™ LDS Sample Buffer (Invitrogen) containing 2.5%  $\beta$ -mercaptoethanol. YFV Asibi infected cells were lysed with 1  $\times$  NuPAGE™ LDS Sample Buffer containing 5%  $\beta$ -mercaptoethanol, and the lysates were heat-inactivated at 70 °C for 15 min. Proteins in the cell lysates were separated on a NuPAGE Novex 4–12% Bis-Tris gel (Invitrogen) and electrophoretically transferred onto a nitrocellulose membrane (Invitrogen). The membranes were blocked with TBST containing 5% nonfat dry milk and probed with the indicated YFV antibodies at 1:1000 dilution. The bound antibodies were visualized with IRDye secondary antibodies (IRDye 800CW Goat anti-Rabbit IgG and IRDye 680RD Goat anti-Mouse IgG) and by imaging with the LI-COR Odyssey system. Mouse monoclonal antibody against  $\beta$ -actin was used as a loading control. A pre-stained protein size marker was purchased from Bio-Rad.

## 2.4. Immunofluorescence assay

Huh-7 cells were seeded on round coverslips (Neuvitro Corporation) in 24-well plates and infected with YFV at 1 multiplicity of infection (MOI) for 24 h. The cells were either fixed with 3.5% paraformaldehyde in PBS at room temperature for 20 min, or 95% ethanol and 5% glacial acetic acid at -20 °C for 10 min, followed by permeabilization with 1% Triton X-100. After blocking with 10% FBS and 2% BSA in PBS for 1 h, the cells were incubated with the corresponding primary antibodies at 4 °C overnight. Subsequently, the cells were washed three times with 0.1% Tween-20 in PBS (PBST) and stained with secondary antibodies. Cell nuclei were counterstained with 4',6-diamidino-2'-phenylindole dihydrochloride (DAPI) purchased from Sigma-Aldrich. Finally, the coverslips were placed on glass slides with ProLong Gold Antifade Mountant (ThermoFisher Scientific). Images were sequentially acquired on an FV1000 confocal microscope with a PlanApoN 60 × /1.42 numerical aperture objective (Olympus).

Primary antibodies against YFV capsid (GTX134022), Envelope (GTX134024), prM (GTX133957), NS1 (GTX134025, GTX134026), NS2B (GTX134028), NS3 (GEX133958, GTX133959) or NS5 (GTX134141) were used at 1:200 dilution. Antibody against NS4B (GTX134030) was used at 1:500 dilution. J2 antibody used for detection of double-stranded RNA was diluted at 1:1000. Alexa Fluor Goat anti-Mouse 488 IgG (H + L) and Alexa Fluor Goat anti-Rabbit 594 IgG (H + L) were used as secondary antibodies at 1:250 dilution.

## 2.5. Visualization of nascent YFV RNA by metabolic incorporation of 5-ethynyl uridine and click chemistry labeling

Huh-7 cells were seeded on round coverslips (Neuvitro Corporation) in 24 well plate and infected with YFV at 1 MOI. At 24 h post infection, cells were treated with 20 μM actinomycin D for 2 h to inhibit the cellular DNA directed RNA transcription, followed by incubation with 1 mM 5-ethynyl uridine (EU; Invitrogen) in the presence of actinomycin D for 1 h. The nascent RNA labeled with EU were visualized by using the Click-iT™ RNA Alexa Fluor™ 594 Imaging Kit (Invitrogen, C10330). Briefly, after fixing cells with 3.5% paraformaldehyde and permeabilization with 1% Triton X-100, “click” reaction between Alexa Fluor labeled azide and EU modified RNA was performed in accordance to the manufacturer’s instructions. Images were acquired on an FV1000 confocal microscope (Olympus) with a PlanApoN 60 × /1.42 numerical aperture objective (Olympus).

## 2.6. Membrane floatation assay

YFV infected cells grown in 60-mm dishes were washed, scraped into PBS, and collected by centrifugation at 500×g for 10 min. After resuspension in 250 μl hypotonic buffer (10 mM Tris-HCl [pH 7.8], 10 mM NaCl) and swelling (15 min on ice), the cells were disrupted by passing through a 27-gauge needle for 25 times. After centrifugation at 900×g for 5 min at 4 °C, the supernatant was mixed with 1.82 ml 72% (wt/wt) sucrose in low-salt buffer (LSB; 50 mM Tris-HCl [pH 7.5], 25 mM KCl, 5 mM MgCl<sub>2</sub>) and overlaid with 2.27 ml of 55% (wt/wt) sucrose in LSB, followed by 0.68 ml of 10% (wt/wt) sucrose in LSB. The sucrose gradient was centrifuged at 46,000 rpm in a Beckman Coulter SW55 ultracentrifuge rotor for 16 h at 4 °C. Ten equal volume (500 μl) fractions were taken sequentially from the top of the gradient. In some experiment, after the primary membrane floatation, the ER-membrane-enriched fraction was collected and divided into equal volume and treated with 1% n-dodecyl β-D-maltoside (DDM; Invitrogen) or 1% digitonin (Promega) for 1 h at 4 °C with rotation. The samples were then mixed with 72% sucrose in LSB and overlaid sequentially with 55% and 10% sucrose to form the gradient and centrifuge as described above. Proteins were precipitated from each fraction by adding 4 vol of methanol followed by centrifugation at 12,000×g for 10 min. Detection of viral and host proteins in each fraction in a Western blot assay was described in

section 2.3.

## 2.7. In-cell western assay

Huh-7 cells were seeded in 96-well plates overnight and infected with YFV at a MOI of 1. At 48 h post-infection, cells were fixed as previously described (Guo et al., 2016; Yu et al., 2012) and probed with YFV NS4B (GTX134030), NS3 (GTX133959) antibodies or anti-Flavivirus Group Antigen antibody 4G2 at 1:1000 dilution. IRDye® 800CW Goat anti-Mouse IgG (LI-COR) or IRDye® 800CW Goat anti-Rabbit IgG were used as secondary antibodies at 1:2000 dilution. Cell viability was determined with DRAQ5 from Biostatus and Sapphire700 from LI-COR. Images and data analysis were obtained using LI-COR Odyssey.

## 2.8. Interferon β promoter reporter assay

293TLR3/IFNβLuc cells were cultured in 96-well black well plates overnight and infected with YFV at a MOI of 0.1. At 48 h post-infection, luciferase activity was analyzed by using an equal volume of luciferase substrate, as previously described (Guo et al., 2014).

## 2.9. Real time RT-PCR

Huh-7 cells were cultured in 24-well plates overnight and infected with YFV at a MOI of 1. At 48 h post-infection, total cellular RNA was extracted using TRIzol Reagent (Thermo Fisher Scientific). YFV RNA was detected in a quantitative reverse transcription-PCR (qRT-PCR) assay using a LightCycler 480II apparatus (Roche). β-actin mRNA served as internal control. Primer sequences are as described previously (Guo et al., 2016).

## 2.10. High-content imaging assay

Huh-7 cells were cultured in 96 or 384-well plates overnight and infected with YFV at the indicated MOI. At 48 h post-infection, cells were fixed with 4% paraformaldehyde and probed with YFV NS4B antibody (GTX134030) at 1:500 dilution. Alexa Fluor Goat anti-Rabbit 594 IgG (H + L) was used as secondary antibody at 1:300. Cell nuclei were stained with DAPI (1:1000). Nine fields per well in 96-well plate, or six fields per well in 384-well plate were taken and analyzed using CellInsight CX7 High-Content Screening Platform (ThermoFisher) to calculate average percent of NS4B positive cells or total immunofluorescence intensity.

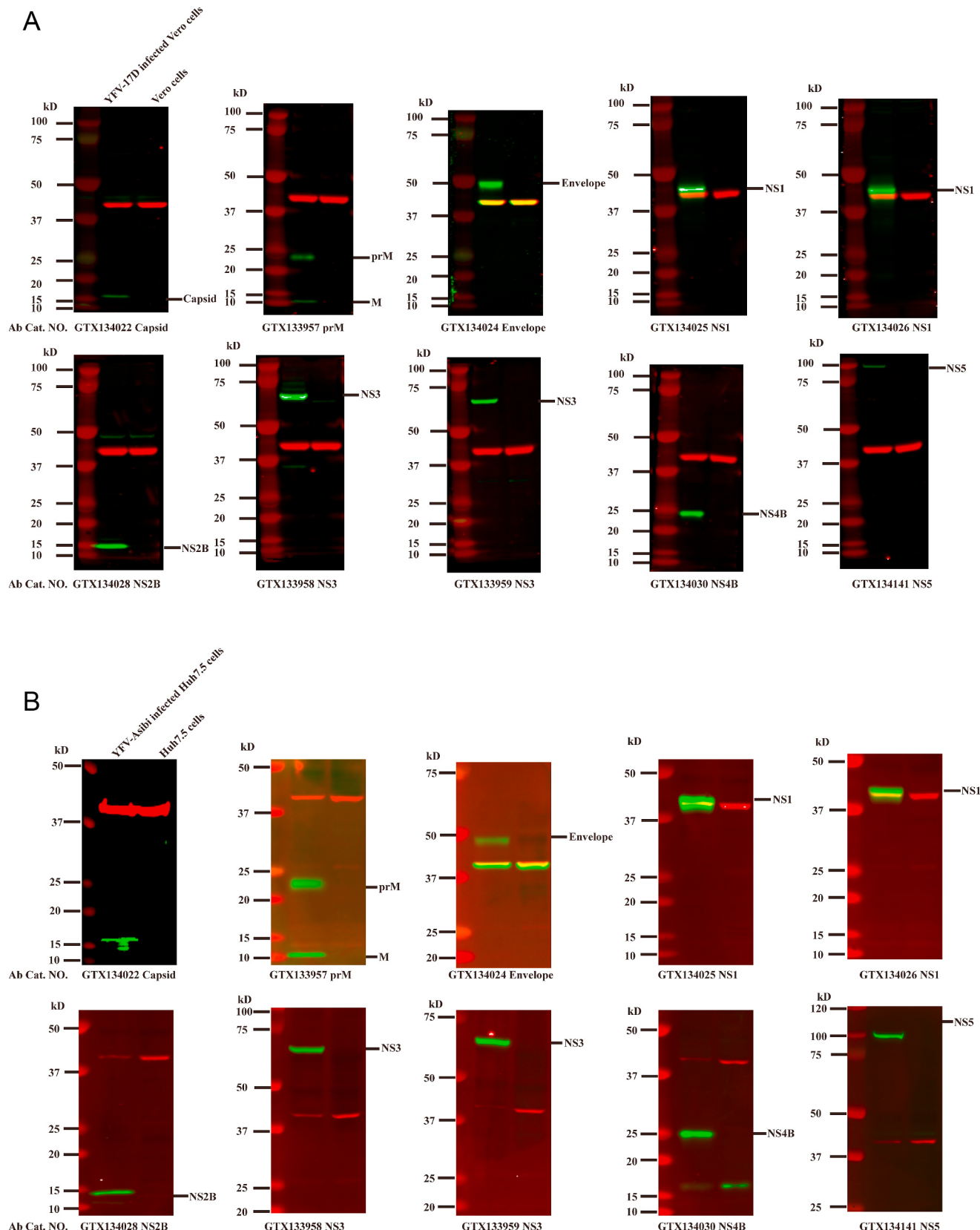
## 2.11. Statistical analysis

Z' factor (Z') was calculated using the following equation:  $Z' = 1 - ((3\delta_p + 3\delta_n)/|\mu_p - \mu_n|)$ , where  $\mu_p$  and  $\mu_n$  are mean values of positive control and negative control, respectively;  $\delta_p$  and  $\delta_n$  are the standard deviations of positive and negative control, respectively (Zhang et al., 1999). Z-score was calculated using the following equation:  $Z\text{-score} = (t - \mu_n)/\delta_n$ , where  $t$  is value of each test well. Other high-throughput screening parameters were determined as described (Liu et al., 2017). P values were calculated using two-tailed Student's t-test. Synergy effect was evaluated using MacSynergy II (Prichard et al., 1993; Prichard and Shipman, 1996).

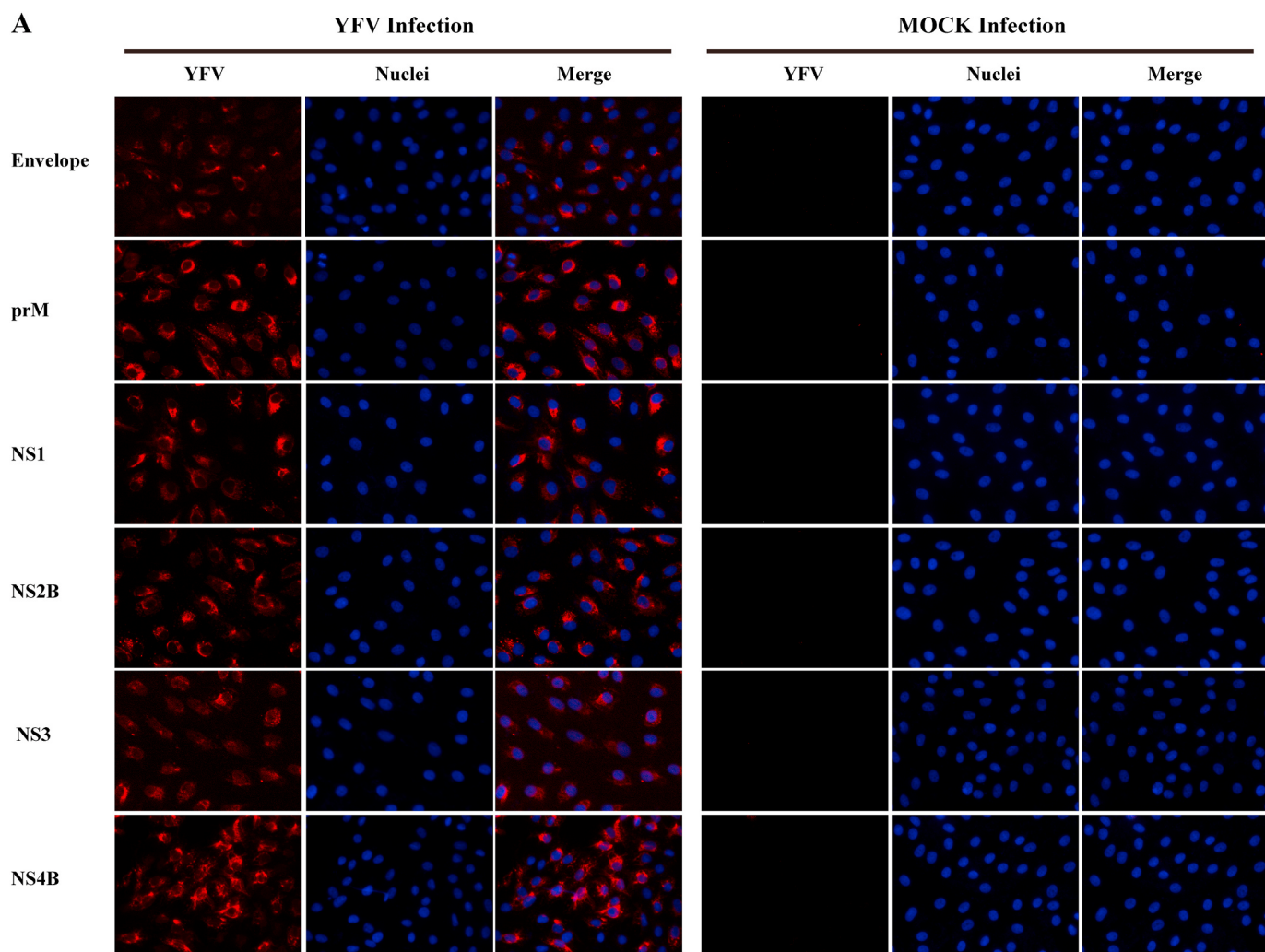
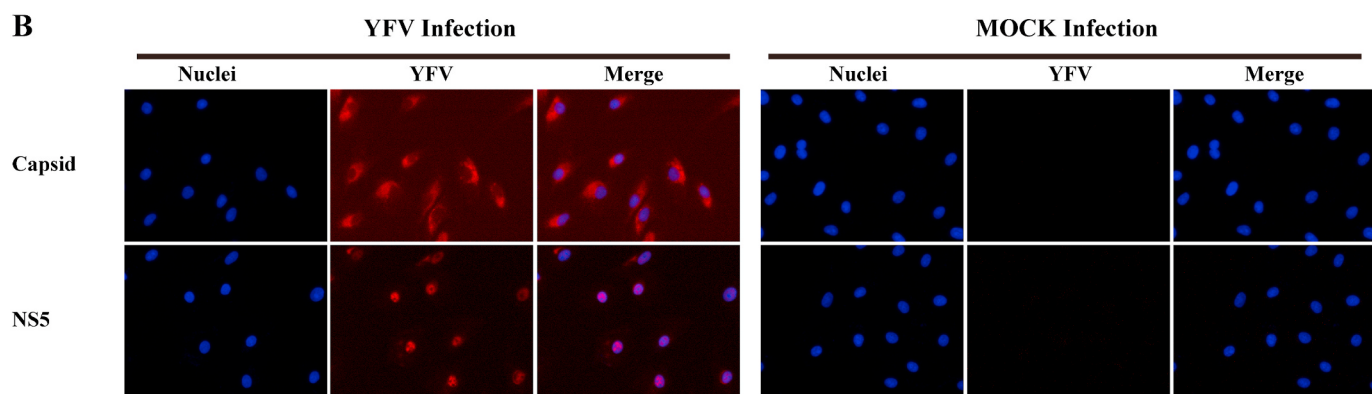
## 3. Results and discussion

### 3.1. Validation of the specificity of rabbit polyclonal antibodies against YFV proteins

A panel of antibodies against all three YFV structural proteins and five of the seven non-structural proteins, including NS1, NS2B, NS3, NS4B and NS5, raised by immunization of rabbits with synthetic peptides or recombinant viral proteins, had become commercially available



**Fig. 1. Detection of YFV structural and non-structural proteins by Western blot assay.** Vero cells were mock-infected or infected with YFV 17D at a MOI of 1 for 48 h (A). Huh-7.5 cells were mock-infected or infected with YFV Asibi at a MOI of 2.5 for 40 h (B). Proteins in the cell lysates were resolved on 4–12% NuPAGE Novex gels and transferred to nitrocellulose membranes. Shown in green are the bands detected after incubation with the indicated rabbit polyclonal primary antibodies against YFV proteins and the IRDye 800CW Goat anti-Rabbit IgG secondary antibody.  $\beta$ -actin, shown in red, is an internal control, and was detected by a mouse monoclonal primary antibody and the IRDye 680RD Goat anti-Mouse IgG secondary antibody. A pre-stained protein molecular weight marker, shown on the left, is used to estimate the size of proteins resolved by gel electrophoresis. The band expected for each of the YFV proteins is indicated on the right.

**A****B**

**Fig. 2. Detection of YFV proteins in YFV-infected cells by immunofluorescence assay.** Huh-7 cells were seeded on 24-well plates and infected with YFV 17D at a MOI of 5 for 24 h. The cells were either fixed with 3.5% paraformaldehyde in PBS at room temperature for 20 min and permeabilized with 1% Triton X-100 (A), or 95% ethanol and 5% glacial acetic acid at -20 °C for 10 min (B). After blocking, the cells were incubated with the indicated primary rabbit polyclonal antibody (NS1 was detected with GTX134025, and NS3 was detected GTX133959) and Alexa Fluor Goat anti-Rabbit 594 IgG (H + L) secondary antibody. Cell nuclei were counterstained with DAPI. Mock-infected cells serve as negative controls. Images were captured by confocal microscopy using a 20 × objective.

from GeneTex, Inc.. The reactivity of these antibodies was initially confirmed by Western blot assays using either recombinant protein or whole cell lysates of 293T cells transiently transfected with a plasmid expressing individual YFV protein, corresponding to the originally used immunogens (<https://www.genetex.com>). In this study, these ten YFV antibodies were further validated by Western blot assays using cell lysates from YFV 17D-infected Vero cells. As shown in Fig. 1A, for the

eight antibodies against YFV capsid, NS1, NS2B, NS3, NS4B or NS5, each detected a single predominant protein species with the expected molecular weight of the corresponding structural or non-structural YFV proteins, only in the YFV-infected cell lysate. Each of the two NS1 antibodies, generated by using recombinant proteins encompassing a sequence within either the center or C-terminal region of YFV NS1 protein, detected a protein species with the same electrophoretic

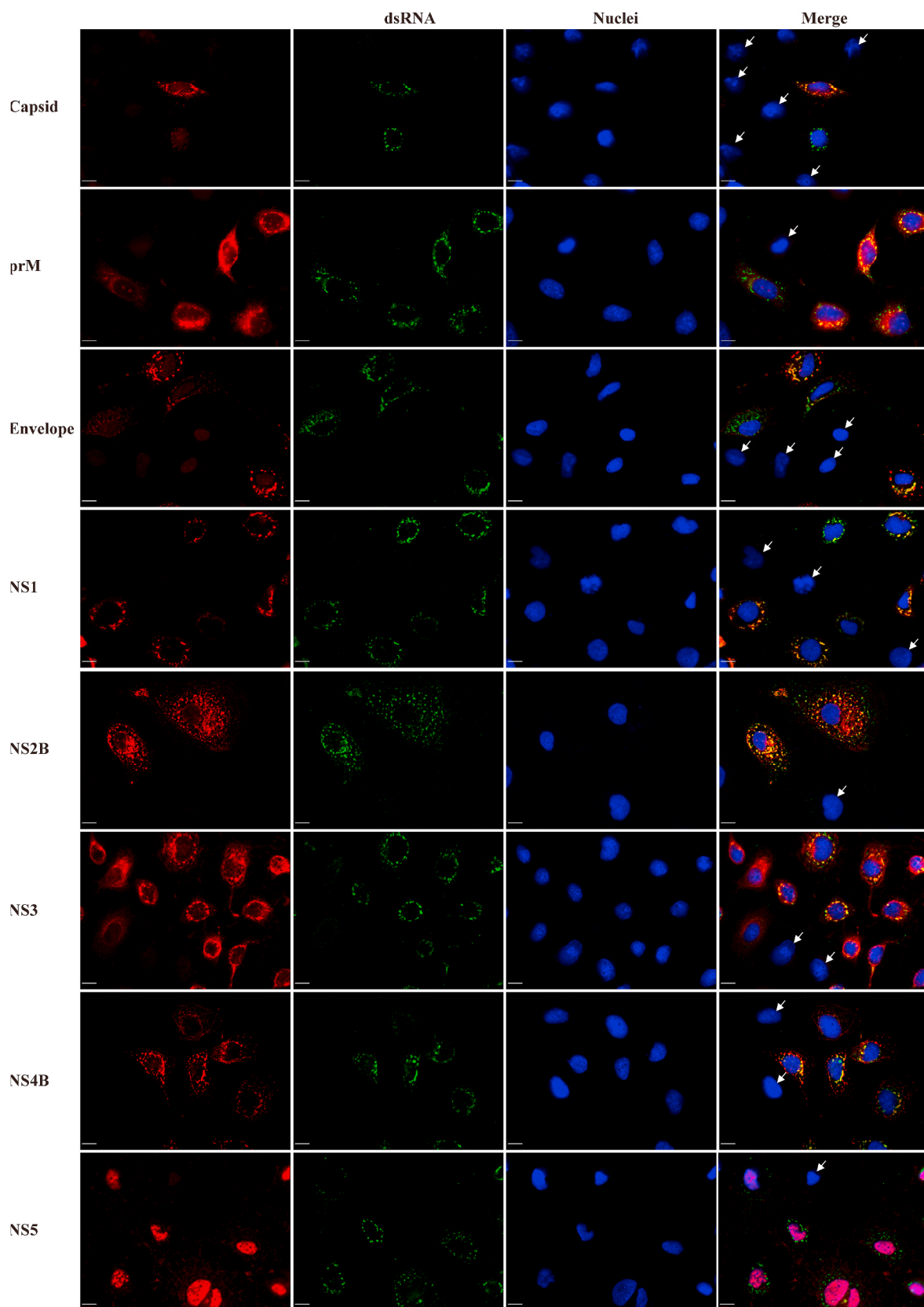


**Fig. 3. Detection of the subcellular localization of YFV proteins and dsRNAs in YFV-infected cells by immunofluorescence assay.** Huh-7 cells were seeded on round coverslips in 24-well plates and infected with YFV 17D at a MOI of 1 for 24 h. The cells were fixed with either 3.5% paraformaldehyde or 95% ethanol and 5% glacial acetic acid as indicated in Fig. 2 legend. YFV proteins were detected by rabbit polyclonal antibodies (NS1 was detected with GTX134025, and NS3 was detected GTX133959) and Alexa Fluor Goat anti-Rabbit 594 IgG (H + L) secondary antibody. dsRNA was detected by mouse monoclonal primary antibody J2 and Alexa Fluor Goat anti-Mouse 488 IgG (H + L). Cell nuclei were counterstained with DAPI. Images were captured by confocal microscopy using a 60 × objective. Scale bar: 100 μM. White arrows indicate uninfected cells.

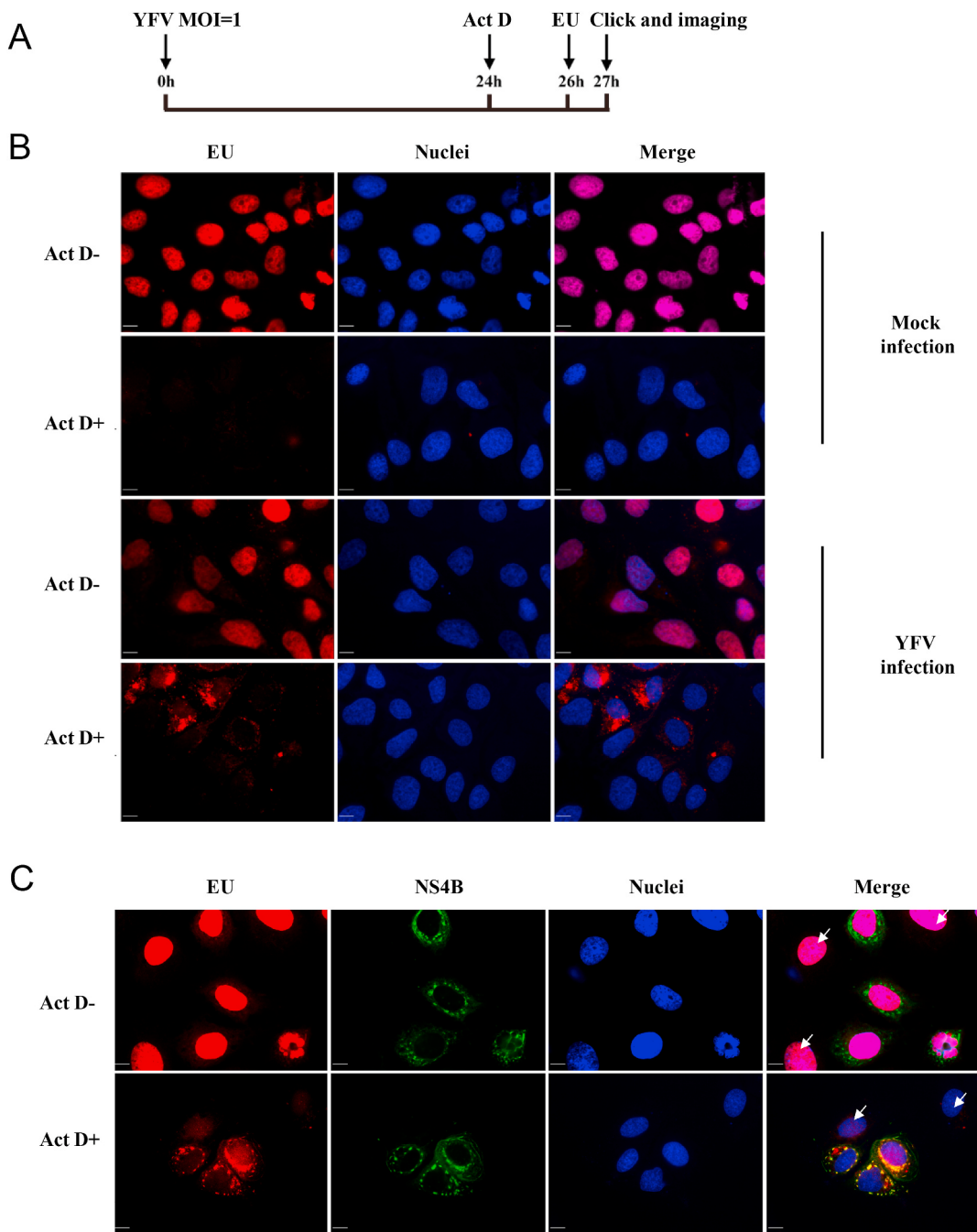


**Fig. 4. Detection of nascent YFV RNA using click chemistry imaging and its co-localization with YFV NS protein.** (A) Schematic illustration of experimental schedule. (B) Huh-7 cells were mock infected or infected with YFV at 1 MOI. 24 h post infection, cells were either mock treated (Act D-) or treated with Actinomycin D (Act D+) for 2 h followed by EU labelling for 1 h. EU labeled nascent RNA was imaged after click reaction with fluorescent labeled azide. (C) Following the click reaction, the localization of YFV NS4B was detected in YFV infected cells as described in Fig. 2. Cell nuclei were counterstained with Hoechst33342. Images were captured by confocal microscopy using a 60 × objective. Scale bar: 100 μM. White arrows indicate uninfected cells.

mobility. Similarly, the two NS3 antibodies, generated by using synthetic peptides encompassing a sequence within either the C-terminus or center region of YFV NS3 protein, also showed comparable sensitivity and specificity in detecting NS3 protein with approximately 69kD. On the contrary, the YFV envelope antibody revealed not only a specific band of approximately 50kD in YFV-infected cell lysates, but also a cross-reacting band that overlaps the β-actin signal in both YFV-infected and uninfected cell lysates, raising concerns for its specificity in recognizing YFV envelope protein in certain assays. The other situation of detecting multiple bands in Western blot assay was observed when prM antibody was used, which only occurred in YFV-infected cells. It is

known that immature flaviviral virions bud into the lumen of the endoplasmic reticulum (ER) and mature in the trans-Golgi network with acidic pH during transportation toward the cell surface (Li et al., 2008). This involves the cleavage of prM protein by cellular furin protease into the “pr” peptide and the M protein (Stadler et al., 1997). Accordingly, the membrane protein of YFV should exist as both immature (prM) and mature (M) forms in the lysate of YFV-infected cells. Because the immunogen for the prM antibody is a synthetic peptide encompassing a sequence in the mature M protein, the antibody thus, as anticipated, recognized both prM and M proteins in the lysates of YFV-infected cells. While the upper band has a size corresponding to prM, the lower weaker

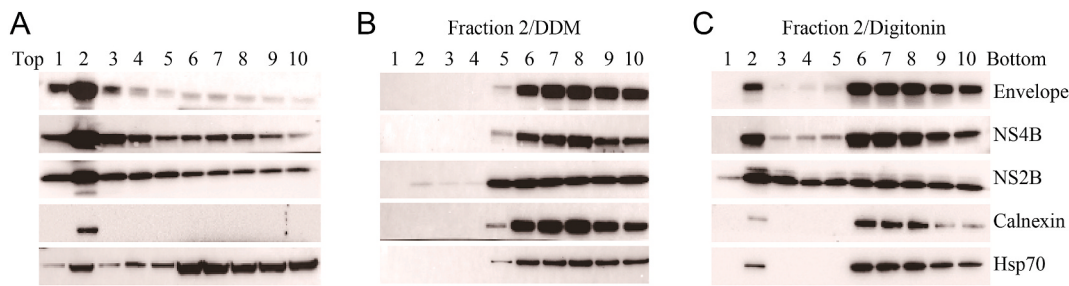


**Fig. 5. Membrane floatation assay to investigate YFV protein interaction and association with cellular membranes.** HEK293 cells infected with YFV at 5 MOI for 24 h were disrupted with hypotonic buffer and overlaid with sucrose gradient. Following centrifugation, 10 fractions were sequentially collected from the top. (A) Proteins extracted from each fraction were analyzed in a Western blot assay to detect indicated YFV envelope and nonstructural proteins, using calnexin and Hsp70 as controls for membrane associated host proteins. (B and C) The fraction containing ER membranes (fraction 2) was collected and subjected to treatment with indicated detergents, followed by a second round of membrane floatation centrifugation in sucrose gradient. Proteins in each fraction were detected by Western blot assays.

band is consistent with M (Zheng et al., 2014).

Sequence alignment of YFV 17D (X03700.1) and a wild-type Asibi strain (KF769016.1) indicated that there are 99% overall homology between the coding region of the two strains. Of the YFV proteins the set of antibodies raised against, the lowest homology is 97.6% in envelope protein, and the highest homology is 100% in capsid protein. To test whether the antibodies can also recognize the corresponding proteins of wild-type YFV, Huh-7.5 cells were infected with YFV Asibi strain at a MOI of 2.5 for 40 h. Flow cytometry using 4G2 antibody indicated that 47% of cells were infected (data not shown). Western blot assays using the cell lysates from uninfected and the wild-type YFV infected Huh-7.5 cells showed that similar to that observed in YFV 17D infected cells, all the antibodies specifically recognized the corresponding wild-type YFV proteins (Fig. 1B).

### 3.2. Intracellular localization of YFV proteins

Next, we examined the ability of these YFV antibodies to detect the corresponding viral proteins in YFV-infected cells using an indirect immunofluorescence assay. Six of the ten antibodies, including the antibodies against envelope, prM, NS1 (GTX134025), NS2B, NS3 (GTX133959), and NS4B, specifically detected individual YFV proteins after the cells were fixed with 3.5% paraformaldehyde and permeabilized with 1% Triton X-100 (Fig. 2A). Two of the antibodies against capsid or NS5 proteins were able to specifically detect the corresponding YFV proteins when the cells were fixed with 95% ethanol and 5% glacial acetic acid (Fig. 2B). All these antibodies displayed a distinct staining pattern that was not seen in uninfected cells. Two additional antibodies against NS1 (GTX134026) and NS3 (GTX133958) failed to detect YFV proteins in YFV-infected cells under the immunofluorescence assay conditions described above. Both of the antibodies were generated using immunogens encompassing sequences in the C-termini of NS1 or NS3, indicating neither of them was exposed under the experimental conditions.

### 3.3. Intracellular distribution of YFV non-structural proteins and their spatial relationship with dsRNA and nascent viral RNA in the cytoplasm

The flavivirus genome replication takes place in the vesicles formed by ER membrane rearrangement induced by the membrane-associated viral nonstructural proteins such as NS4A and NS4B. This process was investigated primarily in DENV-infected cells (Miller et al., 2007; Welsch et al., 2009; Zmurko et al., 2015). We used Huh-7 cells infected with YFV at a MOI of 1 for 24 h so that only a fraction of the cultured cells was infected. An immunofluorescence assay was performed to detect the subcellular localization of the various YFV proteins using confocal microscopy. As shown in Fig. 3, similar to what was reported

for DENV-infected cells, antibodies against the YFV NS proteins (NS1, NS2B, NS3, NS4B) revealed dot-like cytoplasmic structures located in the perinuclear area of infected cells (Miller et al., 2006, 2007; Miller et al., 2007; Miller et al., 2006; Yi et al., 2012). Furthermore, each of the non-structural proteins co-localized with double-stranded RNAs (dsRNAs) (Fig. 3), the putative viral RNA replication intermediates that localize in the replication-hosting vesicles derived from the ER membrane (Welsch et al., 2009; Yi et al., 2011). Previous electron tomography studies of DENV-infected cells revealed that newly synthesized viral RNAs bud through vesicle pores and release of virion particles into the ER lumen occurs in the vicinity of the vesicles (Welsch et al., 2009). Therefore, if a similar replication mechanism holds true for YFV, it is not surprising that some of the dsRNAs also co-localize with structural proteins. An exception is NS5, which, in agreement with previous reports in DENV-infected cells (Miller et al., 2006), localized predominantly in the nuclei of YFV-infected cells. Consistent with its RNA polymerase function, electron tomography has identified DENV NS5 protein also localized in the cytoplasmic vesicles, the presumed sites of flavivirus RNA replication. However, the cytoplasmic DENV NS5 protein is barely detectable by immunofluorescence staining due to its relatively low levels and poor accessibility (Kumar et al., 2013). Similarly, cytoplasmic YFV NS5 protein was also undetectable by the polyclonal YFV NS5 antibody (Fig. 3).

In order to detect viral RNA synthesis *in situ* in infected cells, the nascent viral RNA can also be metabolically labeled by incorporation of unnatural nucleosides, such as 5-ethynyl-2'-uridine (EU), and detected by a click chemistry reaction (Jao and Salic, 2008). This assay allows for the visualization of viral RNA replication foci and determine their spatial relationship with viral and cellular proteins. The experimental procedure is depicted in Fig. 4A. As shown in Fig. 4B, upon the suppression of cellular RNA synthesis by actinomycin D treatment that specifically inhibits DNA-dependent RNA transcription, the RNA-dependent viral RNA synthesis can be specifically detected only in the cytoplasm of YFV infected cells. As anticipated, the cytosolic EU click signals, or the newly synthesized viral RNA, colocalized with NS4B protein (Fig. 4C). Although the click chemistry technologies have been used for studying RNA-dependent viral RNA synthesis in the cells infected with Ebolavirus (Hoenen et al., 2012), chikungunya virus (Reid et al., 2015) or coronavirus (Hagemeijer et al., 2012), this is the first demonstration that this technology can also be used to visualize flavivirus RNA synthesis in infected cells. In conjunction with the immunofluorescent detection of viral nonstructural proteins, the click chemical visualization of intracellular viral RNA synthesis may not only reveal viral and host cellular proteins at viral RNA replication foci, but also provide a powerful tool for *in situ* analyses of viral RNA replication and its inhibition by antiviral drugs.

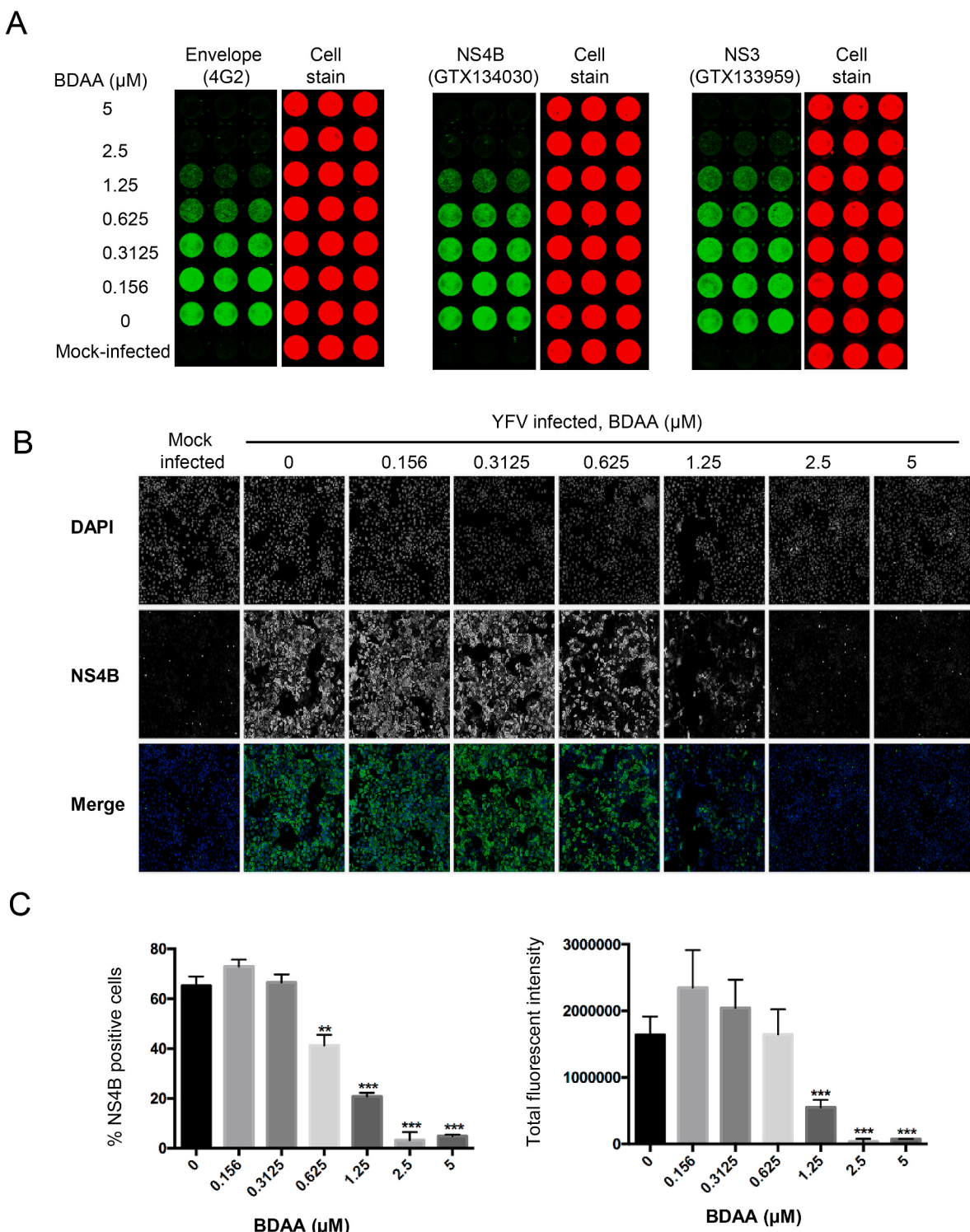


**Fig. 6. Establishment of two YFV NS4B antibody-based antiviral assays.** Huh-7 cells were seeded on 96-well (A) or 384-well plates (B) and infected with YFV 17D at a MOI of 1, with either mock or indicated treatment, for 48 h. (A) In-cell western assay. YFV proteins were detected with indicated antibody against NS3, NS4B or pan-flavivirus monoclonal antibody 4G2 as primary antibody, with IRDye® 800CW goat anti-Rabbit or anti-Mouse as secondary antibodies. Cells were stained with DRAQ5 and Sapphire700. YFV protein expression (green) and cell viability (red) were visualized in LI-COR Odyssey. (B and C) High-content imaging assay. Representative images of NS4B and DAPI staining are shown as a function of doses of BDAA treatment (B). Quantitation of percentage of cells with positive NS4B signal and total fluorescence intensity were calculated based on multiple images taken from each well ( $n = 6$ ) and expressed as average  $\pm$  standard deviation. \* indicates  $P < 0.05$  (C).

### 3.4. Investigation of viral protein association with cellular membranes by membrane flotation assay

Like many positive-stranded RNA viruses, flaviviruses replicate their genomes in the ER-membrane-derived vesicles and assemble progeny virions at ER or ER-Golgi intermediate compartment (ERGIC) membranes. It is, therefore, conceivable that investigating the distribution and interaction of viral proteins and host cellular components at the distinct intracellular membrane compartments is essential to understanding the mechanism of flaviviral genome replication and its inhibition by antiviral agents. To analyze the association of viral and cellular proteins with intracellular membranes, we utilized a membrane flotation assay to separate membrane associated proteins and investigate their interactions with cellular lipids and proteins by a membrane flotation assay through sucrose density gradient ultracentrifugation. As described in Section 2.6 in detail, YFV-infected cells were lysed mechanically in a hypotonic buffer without detergent to preserve cell membranes. The cell lysate was loaded at the bottom of the gradient, overlaid with the lower densities of sucrose solutions. The cellular membranes floated up during the ultracentrifugation to the gradients equivalent to their own density. At the completion of centrifugation, ten equal volume fractions were collected from the top of gradient. The membrane identity and associated proteins in each fraction were analyzed by Western blot assay with antibodies against organelle markers or viral and cellular proteins of interest. As shown in Fig. 5A, as anticipated, viral NS2B, NS4B and envelope proteins were enriched with the ER membrane marker calnexin in fraction 2. Furthermore, treatment of the ER membranes (fraction 2 from the experiment presented in Fig. 5A) with a strong detergent DDM completely disrupted the ER membrane and YFV NS2B, NS4B and envelope proteins were solubilized and distributed into fractions with soluble proteins (Fig. 5B). However, treatment of the ER membranes with the mild detergent digitonin only partially disrupted the membrane and a portion of the viral proteins were still associated with the detergent-resistant membrane structure, presumably lipid rafts, while the vast majority of viral proteins were solubilized under this condition (Fig. 5C). This is consistent with our previous finding that YFV non-structural proteins, presumed to be associated with the replication complex, were associated with detergent resistant membranes (Yi et al., 2012). The lipid rafts-associated viral proteins have been shown to play distinct role in viral genome replication and virion particle morphogenesis at the ER. As has been demonstrated in HCV infected cells, further analysis of YFV viral and host protein-protein interaction in each of these fractions in presence of different detergents, will allow for determination of direct protein interaction or interactions relying on detergent resistant membrane (Boyer et al., 2019). Such study will shed light on the mechanism of virus replication as well as virion morphogenesis in association with various cellular membranes.

### 3.5. Development of antibody-based antiviral assays

The cytopathic effect (CPE)-based cell viability assay, quantification of viral RNA by real time RT-PCR assay, and the plaque-based yield reduction assay are classical analytic tools for quantitative determination of YFV replication and yields (de Freitas et al., 2019; Guo et al., 2016; Liu et al., 2017). A YFV replicon that expresses Renilla luciferase in a replication-dependent manner was also employed for antiviral compound screening (Patkar et al., 2009). Recently, we developed an interferon  $\beta$  promotor-driven-luciferase reporter assay for indirect quantification of viral RNA replication and discovery of antiviral drugs, including YFV (Guo et al., 2014; Ma et al., 2018).

In this study, we modified and/or developed antibody based quantitative YFV antiviral assays. Using two of the YFV antibodies, we modified an in-cell western assay to detect YFV replication, an assay we previously established using the pan-flavivirus envelope antibody 4G2 to detect DENV, ZIKV, and YFV (Guo et al., 2016; Yu et al., 2012) with

**Table 2**  
Antiviral activity of BDAA determined by different assays.

| Assay                            | Measurement                                  | Antiviral activity ( $\mu\text{M}$ ) |                                  |
|----------------------------------|--|--------------------------------------|----------------------------------|
|                                  |  | <sup>f</sup> EC <sub>50</sub>        | <sup>f</sup> EC <sub>90</sub>    |
| Luciferase reporter <sup>a</sup> | YFV activated IFN- $\beta$ promoter activity | 0.47 ±<br>0.02                       | 1.2 ±<br>0.15                    |
| qRT-PCR <sup>b</sup>             | YFV RNA                                      | 0.18 ±<br>0.1                        | 0.28 ±<br>0.05                   |
| Yield reduction <sup>c</sup>     | Viral plaque                                 | 0.32 ±<br>0.15                       | 1.35 ±<br>0.13                   |
| In-cell western <sup>d</sup>     | YFV NS4B/(GTX134030)<br>NS3/(GTX133959)      | 0.78 ±<br>0.11<br>1.10 ±<br>0.06     | 1.75 ±<br>0.27<br>2.42 ±<br>0.17 |
| In-cell western <sup>d</sup>     | YFV envelope/pan flavivirus antibody (4G2)   | 0.6 ±<br>0.04                        | 1.3 ±<br>0.11                    |
| HCI <sup>e</sup>                 | % of YFV NS4B + cells                        | 0.42 ±<br>0.05                       | 0.61 ±<br>0.08                   |

<sup>a</sup> Assay was performed in 293TLR3/IFN $\beta$ Luc cells as previously described (Guo et al., 2014).

<sup>b</sup> Assay was performed in Huh-7 as previously described (Guo et al., 2016).

<sup>c</sup> Assay was performed in Huh-7 cells as previously described (Guo et al., 2016).

<sup>d</sup> Assay was performed in Huh-7 cells as previously described and in Fig. 6A legend (Yu et al., 2012).

<sup>e</sup> Assay was performed in Huh-7 cells as described in Fig. 6B legend.

<sup>f</sup> The EC<sub>50</sub> and EC<sub>90</sub> were obtained by plotting dose response curves and using GraphPad Prism 7.

simultaneous staining of viable cells. As shown in Fig. 6A, the YFV-specific antiviral compound, 2-((S)-3-((S)-sec-butyl)-7-chloro-2-265 oxo-5-phenyl-2,3-dihydro-1H-benzo[e][1,4]diazepin-1-yl)acetic acid (designated as BDAA) (Guo et al., 2016) dose-dependently inhibited YFV infection as judged by a significantly reduced fluorescence intensity revealed by the YFV NS3 and NS4B antibodies with similar result. The same assay was also performed with the 4G2 panflavivirus antibody in parallel, which demonstrated a comparable dose-dependent response with BDAA treatment. Furthermore, a High-Content Imaging (HCI) assay was also established with YFV NS4B antibody-based immunofluorescence staining in combination with image analysis and processing using a CellInsight CX7 High-Content Screening Platform (ThermoFisher). The assay allows for the detection of host cells with DAPI staining as well as with YFV NS4B signal, and automatically analyzes nine fields per sample in 96-well format or six fields per sample in 384-well format. Thus, we can determine the total number of cells and the number of NS4B-positive cells from two images of the same field. Fig. 6B shows representative images and the dose-dependent reduction of NS4B-positive signals following the treatment with antiviral compound BDAA. Fig. 6C shows a quantitative analysis of the images (average of six fields per well in the 384-well plate) using percentage cells with NS4B signal or total immunofluorescence intensity. The two types of analyses reveal a similar dose-dependent response with BDAA treatment.

Next, we validated these two antibody-based antiviral assays by directly comparing them with other well-described assays. As shown in Table 2, similar EC<sub>50</sub> and EC<sub>90</sub> values were obtained using the in-cell western and HCI assays when compared to the interferon  $\beta$  promotor reporter assay, qRT-PCR assay, or yield reduction assay. Each of the previously reported assays has limitations. The interferon  $\beta$  promotor assay can be influenced by innate immune modulatory activity in addition to antiviral activity, while the reliability of the qRT-PCR assay can be affected by viral strain diversity. The yield reduction assay is labor-intensive. These two new YFV antibody based antiviral assays are thus additional tools to quantitatively analyze the molecular events occurring during YFV replication. They should accelerate the discovery of antiviral agents for all the druggable targets, including not only viral components but also cellular factors required for viral replication.

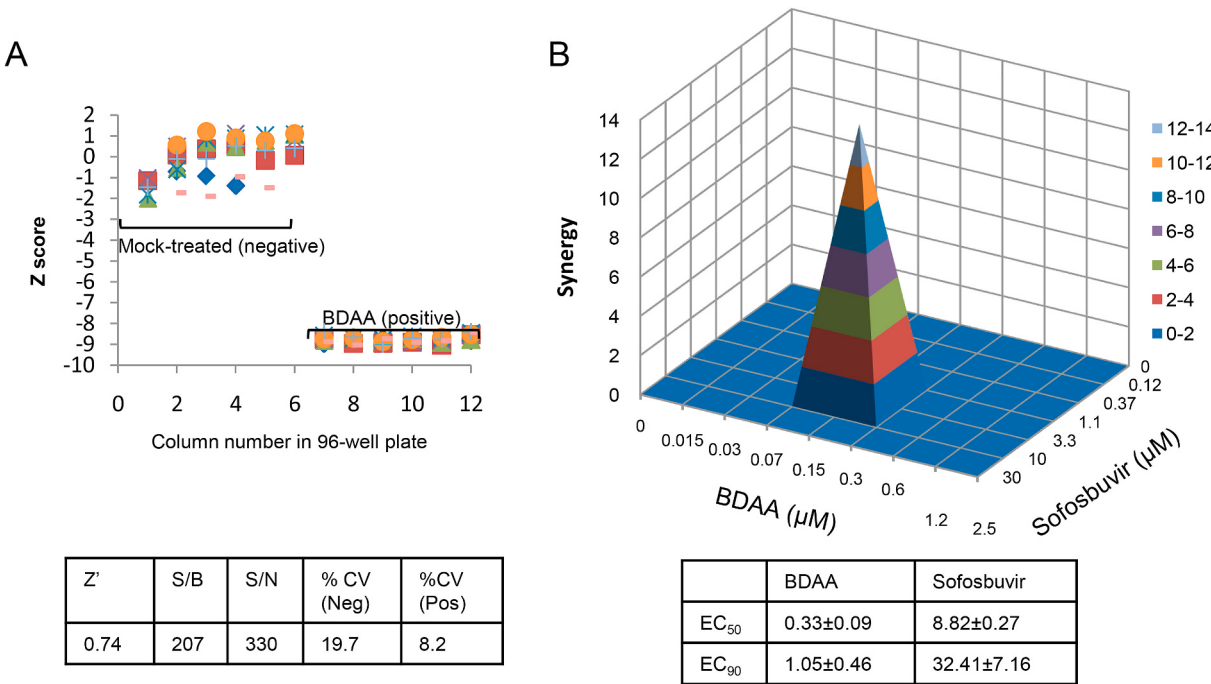


**Fig. 7. Development of high-content imaging-based high-throughput screening assay for YFV.** (A) Huh-7 cells were seeded on 96-well plates and infected with YFV 17D at a MOI of 10 for 48 h. Half of the plate was mock-treated as negative controls, and the other half of the plate was treated with BDAA at 10  $\mu\text{M}$  concentration as positive controls. The average of the percentage of cells with positive NS4B signals from nine fields per well were quantified and used for the calculation of the z-score for each well. Each dot in the plot represents the z-score of a single well in the 96-well plate. Z' value, S/B, S/N and %CV were determined based on the signals from positive and negative control wells. (B) Synergistic effect between BDAA and Sofosbuvir identified using high-content imaging-based HTS assay. Huh-7 cells were seeded on 5 96-well plates and infected with YFV at a MOI of 10 for 1 h. The cells were then treated with the indicated concentrations of each compound or their combinations in a two-dimensional 6  $\times$  8 checkerboard matrix fashion for additional 48 h followed by detection of YFV NS4B and quantification of fluorescent signals (n = 5). The EC<sub>50</sub> values were obtained by plotting mono treatment dose response curves. Synergistic plot was generated using MacSynergy II. The peak above the surface represents synergistic effect with 95% confidence interval.

### 3.6. The high content imaging assay is suitable for high throughput screen of antiviral drugs and evaluation of drug-drug interaction

The HCI assay was also evaluated for its performance as a high-throughput screening platform. As shown in Fig. 7A, while mock-treated wells have z-scores ranging from +2 to -2, the wells treated with BDAA have scores in the range of -8 to -9. Furthermore, using BDAA as a positive control and mock-treated cells as a negative control, the assay has a Z' of 0.74 in YFV-infected Huh-7 cells in a 96-well format. The results suggest that the HCI assay using the YFV NS4B antibody can serve as a high-throughput antiviral screening assay with a cutoff z-score value of -3. As an application of performing the HCI assay in HTS format, we tested the synergistic effect of BDAA that targets YFV NS4B protein and Sofosbuvir, a known nucleoside analog that inhibits YFV NS5 RNA-dependent RNA polymerase. The experiment was performed in five 96-well plates, with serials of nontoxic concentrations of each compound and their combinations in a two-dimensional 6  $\times$  8 checkerboard matrix fashion, with 5 replicates. As shown in Fig. 7B, consistent with published in vitro antiviral data, Sofosbuvir inhibits YFV at EC<sub>50</sub> of 8.82  $\mu\text{M}$  and EC<sub>90</sub> of 32.4  $\mu\text{M}$  (de Freitas et al., 2019). Combination of Sofosbuvir and BDAA, resulted in significant synergistic effect of inhibiting YFV replication, at suboptimal doses of both compounds, between 0.07 and 0.3  $\mu\text{M}$  of BDAA and 1.1–10  $\mu\text{M}$  of Sofosbuvir. This result supports the notion of combination of antivirals targeting two distinct viral proteins to maximize therapeutic benefit.

In conclusion, the studies reported herein demonstrated that the availability of antibodies against eight YFV structural and non-structural proteins greatly facilitate detailed molecular analyses of YFV replication at the sub-cellular levels and provide valuable tools for the identification of key interactions between YFV proteins and host cell factors. The antibody-based assays are also proved invaluable in the screening for,

and elucidation of the mode of action of, novel antiviral compounds against YFV.

### Acknowledgement

Alexander Ball, M.D., GeneTex, Inc., provided technical support and critical reading of the manuscript. This work was partially supported by the National Institutes of Health, USA (AI134732 and AI124690) and the Commonwealth of Pennsylvania through the Hepatitis B Foundation.

### References

- Adungo, F., Yu, F., Kamau, D., Inoue, S., Hayasaka, D., Posadas-Herrera, G., Sang, R., Mwau, M., Morita, K., 2016. Development and characterization of monoclonal antibodies to yellow fever virus and application in antigen detection and IgM capture enzyme-linked immunosorbent assay. *Clin. Vaccine Immunol.* 23, 689–697.
- Beasley, D.W., McAuley, A.J., Bente, D.A., 2015. Yellow fever virus: genetic and phenotypic diversity and implications for detection, prevention and therapy. *Antivir. Res.* 115, 48–70.
- Blight, K.J., McKeating, J.A., Rice, C.M., 2002. Highly permissive cell lines for subgenomic and genomic hepatitis C virus RNA replication. *J. Virol.* 76, 13001–13014.
- Boyer, A., Dreneau, J., Dumans, A., Burlaud-Gaillard, J., Bull-Maurer, A., Roingeard, P., Meunier, J.C., 2019. Endoplasmic reticulum detergent-resistant membranes accommodate hepatitis C virus proteins for viral assembly. *Cells*.
- Bredenbeek, P.J., Kooi, E.A., Lindenbach, B., Huijkman, N., Rice, C.M., Spaan, W.J., 2003. A stable full-length yellow fever virus cDNA clone and the role of conserved RNA elements in flavivirus replication. *J. Gen. Virol.* 84, 1261–1268.
- Calisher, C.H., Woodall, J.P., 2016. Yellow fever-more a policy and planning problem than a biological one. *Emerg. Infect. Dis.* 22, 1859–1860.
- de Freitas, C.S., Higa, L.M., Sacramento, C.Q., Ferreira, A.C., Reis, P.A., Delvecchio, R., Monteiro, F.L., Barbosa-Lima, G., James Westgarth, H., Vieira, Y.R., Mattos, M., Rocha, N., Hoelz, L.V.B., Leme, R.P.P., Bastos, M.M., Rodrigues, G.O.L., Lopes, C.E. M., Queiroz-Junior, C.M., Lima, C.X., Costa, V.V., Teixeira, M.M., Bozza, F.A., Bozza, P.T., Boechat, N., Tanuri, A., Souza, T.M.L., 2019. Yellow fever virus is susceptible to sofosbuvir both in vitro and in vivo. *PLoS Neglected Trop. Dis.* 13, e0007072.

- Douam, F., Ploss, A., 2018. Yellow fever virus: knowledge gaps impeding the fight against an old foe. *Trends Microbiol.* 26, 913–928.
- Douam, F., Ziegler, C.G.K., Hrebikova, G., Fant, B., Leach, R., Parsons, L., Wang, W., Gaska, J.M., Winer, B.Y., Heller, B., Shalek, A.K., Ploss, A., 2018. Selective expansion of myeloid and NK cells in humanized mice yields human-like vaccine responses. *Nat. Commun.* 9, 5031.
- Gaucher, D., Therrien, R., Kettaf, N., Angermann, B.R., Boucher, G., Filali-Mouhim, A., Moser, J.M., Mehta, R.S., Drake 3rd, D.R., Castro, E., Akondy, R., Rinfrat, A., Yassine-Diab, B., Said, E.A., Chouikh, Y., Cameron, M.J., Clum, R., Kelvin, D., Somogyi, R., Greller, L.D., Balderas, R.S., Wilkinson, P., Pantaleo, G., Tartaglia, J., Haddad, E.K., Sekaly, R.P., 2008. Yellow fever vaccine induces integrated multilineage and polyfunctional immune responses. *J. Exp. Med.* 205, 3119–3131.
- Guo, F., Wu, S., Julander, J., Ma, J., Zhang, X., Kulp, J., Cuconati, A., Block, T.M., Du, Y., Guo, J.T., Chang, J., 2016. A novel benzodiazepine compound inhibits yellow fever virus infection by specifically targeting NS4B protein. *J. Virol.* 90, 15.
- Guo, F., Zhao, X., Gill, T., Zhou, Y., Campagna, M., Wang, L., Liu, F., Zhang, P., DiPaolo, L., Du, Y., Xu, X., Jiang, D., Wei, L., Cuconati, A., Block, T.M., Guo, J.T., Chang, J., 2014. An interferon-beta promoter reporter assay for high throughput identification of compounds against multiple RNA viruses. *Antivir. Res.* 107, 56–65.
- Hagemeijer, M.C., Vonk, A.M., Monastyrska, I., Rottier, P.J., de Haan, C.A., 2012. Visualizing coronavirus RNA synthesis in time by using click chemistry. *J. Virol.* 86, 5808–5816.
- Hoenen, T., Shabman, R.S., Groseth, A., Herwig, A., Weber, M., Schudt, G., Dolnik, O., Basler, C.F., Becker, S., Feldmann, H., 2012. Inclusion bodies are a site of ebolavirus replication. *J. Virol.* 86, 11779–11788.
- Jao, C.Y., Salic, A., 2008. Exploring RNA transcription and turnover in vivo by using click chemistry. *Proc. Natl. Acad. Sci. U. S. A.* 105, 15779–15784.
- Julander, J.G., 2013. Experimental therapies for yellow fever. *Antivir. Res.* 97, 169–179.
- Klitting, R., Fischer, C., Drexler, J.F., Gould, E.A., Roiz, D., Paupy, C., de Lamballerie, X., 2018a. What does the future hold for yellow fever virus? (II). *Genes* 9.
- Klitting, R., Gould, E.A., Paupy, C., de Lamballerie, X., 2018b. What does the future hold for yellow fever virus? (I). *Genes* 9.
- Kumar, A., Buhler, S., Selisko, B., Davidson, A., Mulder, K., Canard, B., Miller, S., Bartenschlager, R., 2013. Nuclear localization of dengue virus nonstructural protein 5 does not strictly correlate with efficient viral RNA replication and inhibition of type I interferon signaling. *J. Virol.* 87, 4545–4557.
- Lescar, J., Soh, S., Lee, L.T., Vasudevan, S.G., Kang, C., Lim, S.P., 2018. The dengue virus replication complex: from RNA replication to protein-protein interactions to evasion of innate immunity. *Adv. Exp. Med. Biol.* 1062, 115–129.
- Li, L., Lok, S.M., Yu, I.M., Zhang, Y., Kuhn, R.J., Chen, J., Rossmann, M.G., 2008. The flavivirus precursor membrane-envelope protein complex: structure and maturation. *Science* 319, 1830–1834.
- Lim, S.P., Wang, Q.Y., Noble, C.G., Chen, Y.L., Dong, H., Zou, B., Yokokawa, F., Nilar, S., Smith, P., Beer, D., Lescar, J., Shi, P.Y., 2013. Ten years of dengue drug discovery: progress and prospects. *Antivir. Res.* 100, 500–519.
- Liu, B., Tang, L., Zhang, X., Ma, J., Sehgal, M., Cheng, J., Zhang, X., Zhou, Y., Du, Y., Kulp, J., Guo, J.T., Chang, J., 2017. A cell-based high throughput screening assay for the discovery of cGAS-STING pathway agonists. *Antivir. Res.* 147, 37–46.
- Ma, J., Zhang, X., Soloveva, V., Warren, T., Guo, F., Wu, S., Lu, H., Guo, J., Su, Q., Shen, H., Solon, E., Comunale, M.A., Mehta, A., Guo, J.T., Bavari, S., Du, Y., Block, T. M., Chang, J., 2018. Enhancing the antiviral potency of ER alpha-glucosidase inhibitor IHVR-19029 against hemorrhagic fever viruses in vitro and in vivo. *Antivir. Res.* 150, 112–122.
- Miller, S., Kastner, S., Krijnse-Locker, J., Buhler, S., Bartenschlager, R., 2007. The non-structural protein 4A of dengue virus is an integral membrane protein inducing membrane alterations in a 2K-regulated manner. *J. Biol. Chem.* 282, 8873–8882.
- Miller, S., Sparacio, S., Bartenschlager, R., 2006. Subcellular localization and membrane topology of the Dengue virus type 2 Non-structural protein 4B. *J. Biol. Chem.* 281, 8854–8863.
- Monath, T.P., Vasconcelos, P.F., 2015. Yellow fever. *J. Clin. Virol.* 64, 160–173.
- Patkar, C.G., Larsen, M., Owston, M., Smith, J.L., Kuhn, R.J., 2009. Identification of inhibitors of yellow fever virus replication using a replicon-based high-throughput assay. *Antimicrob. Agents Chemother.* 53, 4103–4114.
- Prichard, M.N., Aseltine, K.R., Shipman Jr., C., 1993. MacSynergy II. Version 1.0. User's Manual. University of Michigan, Ann Arbor.
- Prichard, M.N., Shipman Jr., C., 1996. Analysis of combinations of antiviral drugs and design of effective multidrug therapies. *Antivir. Ther.* 1, 9–20.
- Querec, T.D., Akondy, R.S., Lee, E.K., Cao, W., Nakaya, H.I., Teuwen, D., Pirani, A., Gernert, K., Deng, J., Marzolf, B., Kennedy, K., Wu, H., Bennouna, S., Olouoch, H., Miller, J., Vencio, R.Z., Mulligan, M., Aderem, A., Ahmed, R., Pulendran, B., 2009. Systems biology approach predicts immunogenicity of the yellow fever vaccine in humans. *Nat. Immunol.* 10, 116–125.
- Reid, S.P., Tritsch, S.R., Kota, K., Chiang, C.Y., Dong, L., Kenny, T., Brueggemann, E.E., Ward, M.D., Cazares, L.H., Bavari, S., 2015. Sphingosine kinase 2 is a chikungunya virus host factor co-localized with the viral replication complex. *Emerg. Microb. Infect.* 4, e61.
- Ricciardi-Jorge, T., Bordignon, J., Koishi, A., Zanluca, C., Mosimann, A.L., Duarte Dos Santos, C.N., 2017. Development of a quantitative NS1-capture enzyme-linked immunosorbent assay for early detection of yellow fever virus infection. *Sci. Rep.* 7, 16229.
- Rice, C.M., Lences, E.M., Eddy, S.R., Shin, S.J., Sheets, R.L., Strauss, J.H., 1985. Nucleotide sequence of yellow fever virus: implications for flavivirus gene expression and evolution. *Science* 229, 726–733.
- Stadler, K., Allison, S.L., Schalich, J., Heinz, F.X., 1997. Proteolytic activation of tick-borne encephalitis virus by furin. *J. Virol.* 71, 8475–8481.
- Stock, N.K., Escadafal, C., Achazi, K., Cisse, M., Niedrig, M., 2015. Development and characterization of polyclonal peptide antibodies for the detection of Yellow fever virus proteins. *J. Virol. Methods* 222, 110–116.
- Welsch, S., Miller, S., Romero-Brey, I., Merz, A., Bleck, C.K., Walther, P., Fuller, S.D., Antony, C., Krijnse-Locker, J., Bartenschlager, R., 2009. Composition and three-dimensional architecture of the dengue virus replication and assembly sites. *Cell Host Microbe* 5, 365–375.
- Yi, Z., Sperzel, L., Nurnberger, C., Bredenbeek, P.J., Lubick, K.J., Best, S.M., Stoyanov, C. T., Law, L.M., Yuan, Z., Rice, C.M., MacDonald, M.R., 2011. Identification and characterization of the host protein DNAJC14 as a broadly active flavivirus replication modulator. *PLoS Pathog.* 7, e1001255.
- Yi, Z., Yuan, Z., Rice, C.M., MacDonald, M.R., 2012. Flavivirus replication complex assembly revealed by DNAJC14 functional mapping. *J. Virol.* 86, 11815–11832.
- Yu, W., Gill, T., Wang, L., Du, Y., Ye, H., Qu, X., Guo, J.T., Cuconati, A., Zhao, K., Block, T.M., Xu, X., Chang, J., 2012. Design, synthesis, and biological evaluation of N-alkylated deoxynojirimycin (DNJ) derivatives for the treatment of dengue virus infection. *J. Med. Chem.* 55, 6061–6075.
- Zhang, J.H., Chung, T.D., Oldenburg, K.R., 1999. A simple statistical parameter for use in evaluation and validation of high throughput screening assays. *J. Biomol. Screen* 4, 67–73.
- Zheng, A., Yuan, F., Kleinfelter, L.M., Kielian, M., 2014. A toggle switch controls the low pH-triggered rearrangement and maturation of the dengue virus envelope proteins. *Nat. Commun.* 5, 3877.
- Zmurko, J., Neyts, J., Dallmeier, K., 2015. Flaviviral NS4b, chameleon and jack-in-the-box roles in viral replication and pathogenesis, and a molecular target for antiviral intervention. *Rev. Med. Virol.* 25, 205–223.